J. Fluid Mech. (1987), *vol.* 184, *pp.* 267–288
Printed in Great Britain

A high-order spectral method for the study of nonlinear gravity waves

By DOUGLAS G. DOMMERMUTH AND DICK K. P. YUE

Department of Ocean Engineering, Massachusetts Institute of Technology, Cambridge, MA 02139, USA

(Received 22 December 1986)

We develop a robust numerical method for modelling nonlinear gravity waves which is based on the Zakharov equation/mode-coupling idea but is generalized to include interactions up to an arbitrary order M in wave steepness. A large number ($N = O(1000)$) of free wave modes are typically used whose amplitude evolutions are determined through a pseudospectral treatment of the nonlinear free-surface conditions. The computational effort is directly proportional to N and M, and the convergence with N and M is exponentially fast for waves up to approximately 80% of Stokes limiting steepness ($ka \sim 0.35$). The efficiency and accuracy of the method is demonstrated by comparisons to fully nonlinear semi-Lagrangian computations (Vinje & Brevig 1981); calculations of long-time evolution of wavetrains using the modified (fourth-order) Zakharov equations (Stiassnie & Shemer 1987); and experimental measurements of a travelling wave packet (Su 1982). As a final example of the usefulness of the method, we consider the nonlinear interactions between two colliding wave envelopes of different carrier frequencies.

1. Introduction

The study of the nonlinear dynamics of gravity waves has experienced much progress in the past 20 years. While it is now possible to calculate steep waves even up to overturning (Longuet-Higgins & Cokelet 1976), much of the attention in the past has been devoted to the understanding of weakly nonlinear waves using a variety of perturbation techniques.

A remarkably successful approach for studying slowly modulated waves is the nonlinear Schrödinger equation (NLS) first derived for water waves by Zakharov (1968). By including the leading nonlinearity at third order (in wave slope), NLS predicts salient phenomena such as envelope solitons (Zakharov & Shabat 1972) and recurrence (Yuen & Ferguson 1978). Recently, Dysthe (1979) extended NLS to fourth order which is able to model non-symmetric features such as the unequal growth of sideband perturbations of a Stokes wavetrain, and the forward steepening and fission of wave packets (Lo & Mei 1985). The main shortcomings of NLS are the requirements of narrow-bandedness and slow modulation which render it invalid for many applications – although in the important case of long–short wave interactions, where two or more disparate carrier frequencies are involved, coupled NLS's (which may be derived, for example, via Whitham's 1974 approach using multiple phase functions) may still prove useful. The limitations of NLS in three dimensions are much more severe in that perturbations that are initially confined in a narrow band do not necessarily remain so (Martin & Yuen 1980).

Somewhat more general alternatives to NLS are the so-called Zakharov equations

(Zakharov 1968; Crawford *et al.* 1981) and the closely related mode-coupling approaches (e.g. Phillips 1960; Benney 1962; West, Watson & Thomson 1974; Cohen, Watson & West 1976). These weakly nonlinear theories do not rely on the narrow-banded assumption, and in fact the third-order Zakharov equation contains both the third-order and Dysthe's fourth-order NLS as special cases under the assumption of slow modulation (Stiassnie & Shemer 1984). An indication of the power of the Zakharov equation is its ability to predict remarkable results in two and three dimensions such as linear instability, restabilization at large amplitudes and bifurcations (e.g. Yuen & Lake 1982). For computation of nonlinear wave evolution, the Zakharov equation is discretized in terms of a fixed number of free waves whose amplitudes are governed by coupled nonlinear evolution equations. These differential equations resemble the so-called mode-coupling equations which are obtained by directly substituting a series of Fourier modes into the governing equations and expanding to a given order. In both theories, all the nonlinear interactions among the wave modes are accounted for up to the desired order of accuracy, although owing to computational complexity only a relatively few, say $O(10)$, free waves can typically be used while the number of locked interacting components, or waves locked with the free modes so that they are not themselves governed by evolution equations, can be several orders larger depending on the order of the approximation. While the underlying idea is straightforward, the amount and complexity of the analyses required to extend Zakharov or mode-coupling equations to steeper waves increase rapidly with order. Thus, to date, the Zakharov equation has been modified to include quintet (fourth-order) interactions (Stiassnie & Shemer 1984), and mode-coupling equations have been studied extensively at third order only.

By extending the Zakharov/mode-coupling idea, we develop in this paper a more direct numerical approach for gravity waves whose nonlinearities are not necessarily small. The method computationally accounts for nonlinear interactions up to a specified order M in wave steepness provided that the Taylor series expansion of the velocity potential on the free surface about the mean waterline (cf. (2.4)) remains valid. A large number of free Fourier modes, $N = O(1000)$ in each horizontal dimension, are typically used in our nonlinear simulations. Each of these components is 'free' in that it is subject to its own evolution equation. These modes interact up to the desired order of approximation, and evolve, according to the nonlinear free-surface boundary conditions which we treat in a pseudospectral manner (Fornberg & Whitham 1978). The computational effort increases only linearly with M and, with the use of fast-Fourier transforms, also N. Numerical experiments using exact propagating Stokes waves as benchmark show that the convergence of the results (up to, say, 5 significant figures in surface position, energy, etc.) with respect to N and M is faster than algebraic for intermediate steepnesses. Our experience indicates that $M = O(10)$ is adequate for waves up to approximately 80% of Stokes limiting steepness ($ka \lesssim 0.35$), beyond which convergence is poorer and eventually fails.

To evaluate the accuracy and performance of the present method, we also compare our results to experiments and other theories for three different applications: (*a*) an overturning wave created by an asymmetrically applied surface pressure computed using a fully nonlinear mixed-Eulerian–Lagrangian scheme (MEL) (Longuet-Higgins & Cokelet 1976; Vinje & Brevig 1981); (*b*) the long-time evolution of a two-dimensional wavetrain calculated using the modified (fourth-order) Zakharov equation (Stiassnie & Shemer 1987); and (*c*) experimental measurements of the evolution of a wave envelope packet (Su 1982). The comparisons in all three cases are very

satisfactory. For (*a*), computations can be continued up to close to the breaking point. In both cases (*a*) and (*c*), it is found that as the wave steepens and tends to breaking, the amplitudes of the higher wavenumber components increase. Due to the finite truncation at N, energy is not conserved and the numerical scheme then tends to become unstable. This is manifested by rapid growth in energy of the highest wavenumber modes and the loss of smoothness of the solution. We find that such instabilities can be effectively removed by applying a suitable filter to remove the energy near the truncation region. Surprisingly, this enables us to continue our simulations (and still maintain reasonable agreement) beyond the breaking stages observed in the experiment in (*c*) (see §4.3). In all cases, the apparent onset of wave breaking is marked by a distinct jump in the otherwise conserved total energy curve (e.g. figure 1).

To further illustrate the potential usefulness of the method, we consider as a final example the nonlinear interactions between two colliding wave envelopes of unequal carrier frequencies (§4.4). As expected, the packets emerge largely unaffected except for a shift in position and phase (Longuet-Higgins & Phillips 1962; Zakharov & Shabat 1972; Oikawa & Yajima 1974).

We remark that although our numerical examples here are for deep water in two dimensions only, the present method is quite general and extends readily to three-dimensions and finite-depth (and even shallow water), several computations for which are being carried out and will be reported presently.

2. Mathematical formulation

We consider the irrotational motion of a homogeneous, incompressible and inviscid fluid under a free surface in arbitrary (finite or infinite) depth h. Surface tension is not considered. The origin is located at the mean water level and the vertical axis z is positive upward. For simplicity, the time and mass units are chosen so that the gravitational acceleration and fluid density are unity. The flow can be described by a velocity potential $\Phi(\boldsymbol{x}, z, t)$ such that within the fluid Φ satisfies Laplace's equation. Here $\boldsymbol{x} = (x, y)$ is a vector in the horizontal plane and t is time. Following Zakharov (1968), we define the surface potential

$$\Phi^{\mathrm{S}}(\boldsymbol{x}, t) = \Phi(\boldsymbol{x}, \eta(\boldsymbol{x}, t), t), \tag{2.1}$$

where $z = \eta(\boldsymbol{x}, t)$ denotes the free surface, which we assume to be continuous and single-valued. In terms of Φ^{S}, the kinematic and dynamic boundary conditions on the free surface are respectively

$$\eta_t + \nabla_x \Phi^{\mathrm{S}} \cdot \nabla_x \eta - (1 + \nabla_x \eta \cdot \nabla_x \eta)\, \Phi_z(\boldsymbol{x}, \eta, t) = 0, \tag{2.2a}$$

$$\Phi^{\mathrm{S}}_t + \eta + \tfrac{1}{2} \nabla_x \Phi^{\mathrm{S}} \cdot \nabla_x \Phi^{\mathrm{S}} - \tfrac{1}{2}(1 + \nabla_x \eta \cdot \nabla_x \eta)\, \Phi_z^2(\boldsymbol{x}, \eta, t) = -P_{\mathrm{a}}, \tag{2.2b}$$

where $\nabla_x \equiv (\partial/\partial x, \partial/\partial y)$ denotes the horizontal gradient and P_{a} is the atmospheric pressure. In addition, kinematic boundary conditions are prescribed on body boundaries and the fluid bottom; and for initial conditions, the surface potential $\Phi^{\mathrm{S}}(\boldsymbol{x}, 0)$ and elevation $\eta(\boldsymbol{x}, 0)$ are given.

We assume that Φ and η are $O(\epsilon)$ quantities, where ϵ, a small parameter, is a measure of the wave steepness. We consider a consistent approximation up to and including a given order M in ϵ, and write Φ in a perturbation series in ϵ:

$$\Phi(\boldsymbol{x}, z, t) = \sum_{m=1}^{M} \Phi^{(m)}(\boldsymbol{x}, z, t). \tag{2.3}$$

Here and hereinafter, $(\ )^{(m)}$ denotes a quantity of $O(\epsilon^m)$. We further expand each $\Phi^{(m)}$ evaluated on $z = \eta$ in a Taylor series about $z = 0$, so that from (2.1) we have

$$\Phi^{\mathrm{S}}(x,t) = \Phi(x,\eta,t) = \sum_{m=1}^{M} \sum_{k=0}^{M-m} \frac{\eta^k}{k!} \frac{\partial^k}{\partial z^k} \Phi^{(m)}(x,0,t). \tag{2.4}$$

The validity and convergence of (2.4) is limited by the radius of convergence (from $z = 0$) of Φ, which cannot extend beyond the first singularity in the analytic continuation of Φ above $z = \eta$. In practice, this places the limit on the steepness of the free surface we can consider. At a given instant of time, we may consider Φ^{S} and η known, so that (2.4) is a Dirichlet boundary condition for the unknown Φ. Thus, expanding (2.4) and collecting terms at each order, we obtain a sequence of boundary conditions for the unknown $\Phi^{(m)}$'s on $z = 0$:

$$\Phi^{(m)}(x,0,t) = R^{(m)}, \quad m = 1,2,\ldots,M, \tag{2.5a}$$

where $R^{(1)} = \Phi^{\mathrm{S}}$

and $$R^{(m)} = -\sum_{k=1}^{m-1} \frac{\eta^k}{k!} \frac{\partial^k}{\partial z^k} \Phi^{(m-k)}(x,0,t), \quad m = 2,3,\ldots,M. \tag{2.5b}$$

These boundary conditions, in addition to Laplace's equation and appropriate body and bottom boundary conditions etc., define a sequence of boundary-value problems for $\Phi^{(m)}$, $m = 1,2,\ldots,M$, in the domain $z \leqslant 0$. These problems can be solved successively at increasing orders for any prescribed Φ^{S} and η.

As in a typical mode-coupling approach, we represent each $\Phi^{(m)}$ as an eigenfunction expansion of free modes which satisfy all but the Dirichlet free-surface conditions (2.5). Thus we write

$$\Phi^{(m)}(x,x,t) = \sum_{n=1}^{\infty} \Phi_n^{(m)}(t)\, \Psi_n(x,z), \quad z \leqslant 0, \tag{2.6}$$

where, in practice, the number of eigenmodes is truncated at some suitable number N. Substitution of (2.6) into (2.5) determines the amplitudes $\Phi_n^{(m)}(t)$ in terms of the modal components of Φ^{S}. Our main objective is the surface vertical velocity

$$\Phi_z(x,\eta,t) = \sum_{m=1}^{M} \sum_{k=0}^{M-m} \frac{\eta^k}{k!} \sum_{n=1}^{N} \Phi_n^{(m)}(t) \frac{\partial^{k+1}}{\partial z^{k+1}} \Psi_n(x,0), \tag{2.7}$$

which, when substituted into the free-surface conditions (2.2) yields the final result

$$\left.\begin{aligned} &\eta_t + \nabla_x \Phi^{\mathrm{S}} \cdot \nabla_x \eta - (1 + \nabla_x \eta \cdot \nabla_x \eta)\left[\sum_{m=1}^{M} \sum_{k=0}^{M-m} \frac{\eta^k}{k!} \sum_{n=1}^{N} \Phi_n^{(m)}(t) \frac{\partial^{k+1}}{\partial z^{k+1}} \Psi_n(x,0)\right] = 0, \\ &\Phi_t^{\mathrm{S}} + \eta + \tfrac{1}{2} \nabla_x \Phi^{\mathrm{S}} \cdot \nabla_x \Phi^{\mathrm{S}} - \tfrac{1}{2}(1 + \nabla_x \eta \cdot \nabla_x \eta) \\ &\qquad \times \left[\sum_{m=1}^{M} \sum_{k=0}^{M-m} \frac{\eta^k}{k!} \sum_{n=1}^{N} \Phi_n^{(m)}(t) \frac{\partial^{k+1}}{\partial z^{k+1}} \Psi_n(x,0)\right]^2 = -P_{\mathrm{a}}. \end{aligned}\right\} \tag{2.8}$$

Equations (2.8) are the evolution equations for Φ^{S} and η in terms of the modal amplitudes $\Phi_n^{(m)}$, which themselves are given by the values of these surface quantities according to (2.5), and the problem is complete. We point out that (2.8) is the generalization to Mth order in wave steepness of the perturbation equations which form the basis of mode-coupling formulations (e.g. West 1982, Appendix A).

In a variation to the present approach the expansions (2.3) and (2.4) are avoided, the eigenfunctions Ψ_n are continued above $z = 0$, and (2.1) is written directly as

$$\Phi(\boldsymbol{x}, \eta, t) = \sum_{n=1}^{N} \Phi_n(t)\, \Psi_n(\boldsymbol{x}, \eta) = \Phi^{\mathrm{S}}(\boldsymbol{x}, t). \tag{2.9a}$$

The corresponding expressions for the evolution equations (2.8) are

$$\left.\begin{aligned} \eta_t + \nabla_x \Phi^{\mathrm{S}} \cdot \nabla_x \eta - (1 + \nabla_x \eta \cdot \nabla_x \eta) \sum_{n=1}^{N} \Phi_n(t) \frac{\partial}{\partial z} \Psi_n(\boldsymbol{x}, \eta) = 0, \\ \Phi_t^{\mathrm{S}} + \eta + \tfrac{1}{2} \nabla_x \Phi^{\mathrm{S}} \cdot \nabla_x \Phi^{\mathrm{S}} - \tfrac{1}{2}(1 + \nabla_x \eta \cdot \nabla_x \eta) \left[\sum_{n=1}^{N} \Phi_n(t) \frac{\partial}{\partial z} \Psi_n(\boldsymbol{x}, \eta) \right]^2 = -P_{\mathrm{a}}. \end{aligned}\right\} \tag{2.9b}$$

By collocating (2.9a) at discrete points $\boldsymbol{x}_j$ on the exact free surface, the modal amplitudes are obtained as solutions of a system of algebraic equations. Examples of this method include Rienecker & Fenton (1981) who performed the collocation in physical space, and Bryant (1983) who collocated in Fourier space. For deep water, $\Psi_n \approx \exp(nz)$, say, and for maximum and minimum surface elevation $\eta_{\max}$ and $\eta_{\min}$ respectively, the ratio $|\Psi_n(\boldsymbol{x}, \eta_{\max}) / \Psi_n(\boldsymbol{x}, \eta_{\min})|$ increases rapidly with n for finite ϵ. As N increases, the conditioning of the equation system deteriorates severely, independent of the convergence of (2.4). Moreover, the operation count is typically $O(N^3)$ per time step. Thus, the present scheme using (2.5) may be viewed as an effective and efficient perturbation solution of the system (2.9a).

In the special case of shallow water, $h \ll 1$, we may choose to expand $\Phi(\boldsymbol{x}, z, t)$ about $z = -h$ instead. As a result, the series (2.7) for the vertical velocity can be summed explicitly, and the evolution equations (2.8) may be written in closed form as

$$\left.\begin{aligned} \eta_t + \nabla_x \Phi^{\mathrm{S}} \cdot \nabla_x \eta + (1 + \nabla_x \eta \cdot \nabla_x \eta)\, \mathrm{TAN}\,[(\eta + h) \nabla_x] \nabla_x \Phi^{\mathrm{S}} = 0, \\ \Phi_t^{\mathrm{S}} + \eta + \tfrac{1}{2} \nabla_x \Phi^{\mathrm{S}} \cdot \nabla_x \Phi^{\mathrm{S}} - \tfrac{1}{2}(1 + \nabla_x \eta \cdot \nabla_x \eta) \{\mathrm{TAN}\,[(\eta + h) \nabla_x] \nabla_x \Phi^{\mathrm{S}}\}^2 = -P_{\mathrm{a}}, \end{aligned}\right\} \tag{2.10a}$$

where the tangent operator denotes the sum

$$\begin{aligned} &\mathrm{TAN}\,[(\eta + h) \nabla_x] \nabla_x \Phi^{\mathrm{S}} \\ &\qquad = (\eta + h) \nabla_x^2 \Phi^{\mathrm{S}} + \tfrac{1}{3}(\eta + h)^3 \nabla_x^4 \Phi^{\mathrm{S}} + \ldots, \quad |(\eta + h) \nabla_x| \leqslant \tfrac{1}{2}\pi. \end{aligned} \tag{2.10b}$$

In order for the perturbation series to be convergent, the inequality in (2.10b) places a limit on the maximum horizontal wavenumber (and hence a maximum for the mode number N) relative to $(\eta + h)$ that can be used. Thus, for a given surface distribution Φ^{S}, there is an upper bound on the resolution that can be achieved in the context of the shallow-water equations (2.10).

For simple geometries, the eigenfunctions in (2.6) are readily available. For 2π-periodic boundary conditions in (x, y), say, (2.6) can be represented as

$$\Phi^{(m)}(\boldsymbol{x}, z, t) = \sum_{n=0}^{\infty} \Phi_n^{(m)}(t) \exp\left[|\boldsymbol{\kappa}_n| z + \mathrm{i} \boldsymbol{\kappa}_n \cdot \boldsymbol{x}\right] \tag{2.11}$$

for deep water, and for constant finite depth h,

$$\Phi^{(m)}(\boldsymbol{x}, z, t) = \sum_{n=0}^{\infty} \Phi_n^{(m)}(t) \frac{\cosh\left[|\boldsymbol{\kappa}_n| (z + h)\right]}{\cosh\left(|\boldsymbol{\kappa}_n| h\right)} \exp\left(\mathrm{i} \boldsymbol{\kappa}_n \cdot \boldsymbol{x}\right). \tag{2.12}$$

Here, $\boldsymbol{\kappa}_n = (k_x, k_y)$ is the wavenumber vector, and the summation in n implies summing over all integer values of k_x and k_y including the complex-conjugate terms.

The analysis is slightly more complicated for a mildly varying bottom given by $z = -h+\zeta(\boldsymbol{x}, t)$, for example. The kinematic condition on the bottom is

$$\zeta_t + \nabla_x \zeta \cdot \nabla_x \Phi - \Phi_z = 0, \quad \text{on } z = -h+\zeta. \tag{2.13}$$

For a mean depth h and a variation $\zeta = O(\epsilon)$, a two-term expansion for $\Phi^{(m)}$ can be used:

$$\Phi^{(m)} = \alpha^{(m)} + \beta^{(m)}, \tag{2.14a}$$

where $\alpha^{(m)}$ is as given by (2.12), and $\beta^{(m)}$ satisfies zero Dirichlet condition on $z = 0$:

$$\beta^{(m)}(\boldsymbol{x}, z, t) = \beta_0^{(m)}(t) z + \sum_{n=1}^{\infty} \beta_n^{(m)}(t) \frac{\sinh(|\boldsymbol{\kappa}_n| z)}{|\boldsymbol{\kappa}_n| \cosh(|\boldsymbol{\kappa}_n| h)} \exp(\mathrm{i}\boldsymbol{\kappa}_n \cdot \boldsymbol{x}). \tag{2.14b}$$

The sequence of equations corresponding to (2.5) in terms of $\alpha^{(m)}$ and $\beta^{(m)}$ is, upon substitution:

$$\left.\begin{aligned} \alpha^{(1)} &= \Phi^{\mathrm{S}}, && \text{on } z = 0, \\ \beta_z^{(1)} &= \frac{\partial \zeta}{\partial t}, && \text{on } z = -h, \\ \alpha^{(2)} &= -\eta(\alpha^{(1)} + \beta^{(1)})_z, && \text{on } z = 0, \\ \beta_z^{(2)} &= -\zeta(\alpha^{(1)} + \beta^{(1)})_{zz} + \nabla_x \zeta \cdot \nabla_x (\alpha^{(1)} + \beta^{(1)}), && \text{on } z = -h. \end{aligned}\right\} \tag{2.15}$$

etc....

The evaluation of the vertical velocity and the free-surface evolution equation follows as before. For more complex boundaries (such as bodies), the set of eigenfunctions may be obtained by direct numerical means. The boundary-value problems for $z \leqslant 0$ are in general linear, and for boundaries not moving more than $O(\epsilon)$ in time, need to be solved only once.

3. Numerical method

3.1. *Implementation*

The numerical method for a problem using N wave modes and retaining nonlinearities up to a specified order M consists of two parts:

(*a*) Given the surface elevation $\eta(\boldsymbol{x}, t)$ and potential $\Phi^{\mathrm{S}}(\boldsymbol{x}, t)$ on that surface at some instant of time t, the modal amplitudes of the velocity potential $\Phi_n^{(m)}(t)$ subject to the Dirichlet condition (2.4) are solved using a pseudospectral method. Specifically, all spatial derivatives of $\Phi^{(m)}$, Φ^{S} and η are evaluated in eigenfunction (wavenumber) space while nonlinear products are calculated in physical space at a discrete set of points $\boldsymbol{x}_j$. For periodic boundary conditions where the eigenfunction expansions are represented as Fourier series (2.11, 2.12 and 2.14), $\boldsymbol{x}_j$ are equally spaced and fast-Fourier transforms are used to project between the wavenumber and physical domains. At each order, (2.5) is solved in wavenumber space by equating Fourier modes, and the number of operations required is $O(N \ln N)$. For perturbations up to order M the operation count is then $O(MN \ln N)$ per time step.

(*b*) The evolution equations (2.8) are then integrated in time to obtain the new values $\eta(\boldsymbol{x}, t+\Delta t)$ and $\Phi^{\mathrm{S}}(\boldsymbol{x}, t+\Delta t)$. For our present computations, we use a fourth-order Runge–Kutta integrator with constant time step Δt.

The two-step procedure (*a*)–(*b*) is repeated starting from initial conditions.

3.2. *Error considerations*

There are four main sources of computational errors:

3.2.1. *Errors due to truncation in the number of modes N and order M*

For sufficiently smooth η and Φ^S the coefficients $\Phi_n^{(m)}$ of an orthogonal eigen function expansion vanish more rapidly than any algebraic power of n as $n \to \infty$. Similarly, for mild nonlinearities, the truncation error after order M is $O(\epsilon^{M+1})$, and converges exponentially fast as M increases. As is pointed out after (2.4), such convergence ceases beyond certain wave steepnesses owing to singularities in the analytic continuation of the velocity potential. These observations are substantially confirmed in our numerical tests for Stokes waves (see §3.3) where the critical steepness is found to be $\epsilon = ka \approx 0.35$.

3.2.2. *Amplification of round-off errors*

The integrity of the numerical results can be severely limited by the amplification of computational errors. Consider, for instance, a small random error δ_{mn} in the amplitude $\Phi_n^{(m)}$, i.e. $\Phi_n^{(m)} = \tilde{\Phi}_n^{(m)}(1+\delta_{mn})$, where the tilde denotes 'exact' values. The error in $R^{(m)}$, (2.5*b*), after using (2.6) is then given by

$$R^{(m)} - \tilde{R}^{(m)} = -\sum_{k=1}^{m-1} \frac{\eta^k}{k!} \sum_{n=1}^{N} \tilde{\Phi}_n^{(m-k)} \delta_{(m-k),n} \frac{\partial^k}{\partial z^k} \Psi_n. \tag{3.1}$$

In general, $|\partial^k/\partial z^k \Psi_n| \approx |\kappa_n|^k$, while $|\kappa_n| \approx n$, say, so that at any order the error in the highest wavenumber modes is the most amplified. This is probably a root cause of unstable growth of errors in many nonlinear free-surface simulations where large wavenumbers (or fine spatial resolutions) are used. Notable exceptions include Vinje & Brevig (1981) and also Dold & Peregrine (1986). To eliminate such high-wavenumber instabilities, we follow Longuet-Higgins & Cokelet (1976) and apply a smoothing function to η and Φ^S. Their five-point smoothing function can be effectively applied in wavenumber space which is equivalent to the low-pass filter

$$\Lambda(\kappa_n) = \frac{1}{8}\left[5 + 4\cos\left(\frac{\pi|\kappa_n|}{|\kappa_N|}\right) - \cos\left(\frac{2\pi|\kappa_n|}{|\kappa_N|}\right)\right]. \tag{3.2}$$

Alternatively, we may simply use an ideal low-pass filter:

$$\Lambda_I(\kappa_n, \nu) = \begin{cases} 1 & \text{for } |\kappa_n|/|\kappa_N| \leqslant \nu \\ 0 & \text{for } |\kappa_n|/|\kappa_N| > \nu \end{cases} \quad 0 < \nu \leqslant 1. \tag{3.3}$$

It is useful to compare the areas under these filters

$$\int \Lambda(\kappa) \mathrm{d}\kappa \Big/ \int \Lambda_I(\kappa, \nu)\, \mathrm{d}\kappa = \frac{5}{8\nu}, \tag{3.4}$$

which indicates that Λ_I would remove less energy than Λ if $\nu > \frac{5}{8}$. Since the ideal filter does not affect the lower wavenumbers, (3.3) is often preferred. In many simulations no smoothing or filtering is necessary. We point out that a useful alternative when modelling physical experiments may be to introduce wavenumber-dependent damping terms explicitly in the spectral equations. This is, however, not applied in the present work.

3.2.3. *Aliasing errors*

Consider the product $h(x)$ of two functions $f(x)$ and $g(x)$ and their respective Fourier series representations:

$$h(x) = \sum_{n=-N}^{N} h_n \, e^{inx}; \quad f(x) = \sum_{n=-N}^{N} f_n \, e^{inx}; \quad g(x) = \sum_{n=-N}^{N} g_n \, e^{inx}.$$

In our pseudospectral application, the product is performed in physical space at equally spaced points x_j: $h(x_j) = f(x_j)\, g(x_j)$. Whereupon we have

$$h_n = \sum_{j+k=n} f_j g_k + \sum_{j+k=n\pm N} f_j g_k, \quad j,k = 0, \pm 1, \pm 2, \ldots, \pm N. \tag{3.5}$$

The second sum represents the aliasing error terms which arise whenever $j+k = n$ (modulo N). It is well known (e.g. Orszag 1971) that the best approximation to the product in the mean-square sense is the so-called alias-free sum. To obtain this, we double the number of modes (and the number of collocation points x_j) for each function. Thus, we define new functions $\tilde{h} = \tilde{f}\tilde{g}$, where

$$\tilde{h}(x) = \sum_{n=-2N}^{2N} \tilde{h}_n \, e^{inx}; \text{ etc.}$$

and $(\tilde{f}_n, \tilde{g}_n) = (f_n, g_n)$ for $|n| \leqslant N$, and $\tilde{f}_n, \tilde{g}_n = 0$ for $N < |n| \leqslant 2N$. The Fourier coefficients of the alias-free sum h are then given by $h_n = \tilde{h}_n$ for $|n| \leqslant N$. For products involving two or more terms, the multiplication is done successively where each factor is made alias-free before multiplying by the next term. In general, for N alias-free modal degrees of freedom, $2N$ complex-conjugate pairs of Fourier coefficients must be used.

3.2.4. *Errors due to numerical time integration*

The local truncation error of the fourth-order Runge–Kutta (RK4) scheme that we use to integrate the evolution equations (2.8) is $O(\Delta t^5)$. The global truncation error for $t = O(1)$ is fourth order in Δt (see table 2). RK4 requires twice as many evaluations as the commonly used fourth-order multi-step Adams–Bashforth–Moulton (ABM4) method, but has a somewhat lower global truncation error and a larger stability region. Using a linearized stability analysis, the Courant condition for RK4 is $\Delta t^2 \leqslant 8/|\kappa_N|$, which should also be a necessary condition for the nonlinear problem. In contrast, ABM4 is weakly unstable for any Δt according to linear stability analysis.

3.3. *Numerical convergence tests*

We test the accuracy and convergence (with respect to N, M and Δt) of our method using exact (progressive) Stokes waves as benchmark. For the solution of the latter, we follow Schwartz (1974) but solve the nonlinear equations associated with the mapping function (Schwartz' equations 2.6) directly using Newton iteration rather than high-order perturbation. The final results are exact to 14 significant figures. For simplicity, we consider deep water where, for a wavelength of 2π, the eigenfunctions are given by (2.11) with integer wavenumbers $\kappa_n = (n, 0)$, $n = 0, \pm 1, \pm 2, \ldots, \pm N$. The numerical tests consist of two parts:

3.3.1. *Convergence of the boundary-value problem solution*

This corresponds to step (*a*) of §3.1 where here we prescribe η and Φ^S from exact Stokes waves and solve (2.5) for the velocity potential. In particular we compare the surface vertical velocity $\Phi_z|_{z=\eta}$ against the exact value.

		M						
ϵ	N	2	4	6	8	10	12	14
0.1	8	0.75×10^{-3}	0.68×10^{-5}	0.72×10^{-7}	0.22×10^{-8}	0.10×10^{-8}		
	16	0.75×10^{-3}	0.68×10^{-5}	0.65×10^{-7}	0.64×10^{-9}	0.49×10^{-10}		
0.2	8	0.59×10^{-2}	0.22×10^{-3}	0.15×10^{-4}	0.18×10^{-5}	0.13×10^{-5}		
	16	0.60×10^{-2}	0.22×10^{-3}	0.87×10^{-5}	0.37×10^{-6}	0.38×10^{-7}		
	32	0.60×10^{-2}	0.22×10^{-3}	0.88×10^{-5}	0.35×10^{-6}	0.14×10^{-7}	0.75×10^{-9}	
0.3	8	0.19×10^{-1}	0.22×10^{-2}	0.47×10^{-3}	0.14×10^{-3}	0.16×10^{-3}		
	16	0.20×10^{-1}	0.18×10^{-2}	0.19×10^{-3}	0.59×10^{-4}	0.24×10^{-4}		
	32	0.20×10^{-1}	0.18×10^{-2}	0.17×10^{-3}	0.16×10^{-4}	0.17×10^{-5}		
	64	0.20×10^{-1}	0.18×10^{-2}	0.17×10^{-3}	0.16×10^{-4}	0.16×10^{-5}	0.21×10^{-6}	0.33×10^{-7}
0.35	8	0.31×10^{-1}	0.64×10^{-2}	0.22×10^{-2}	0.13×10^{-2}	0.13×10^{-2}		
	16	0.31×10^{-1}	0.41×10^{-2}	0.99×10^{-3}	0.71×10^{-3}	0.22×10^{-3}		
	32	0.31×10^{-1}	0.40×10^{-2}	0.53×10^{-3}	0.94×10^{-4}	0.95×10^{-4}	0.16×10^{-3}	
	64	0.31×10^{-1}	0.40×10^{-2}	0.53×10^{-3}	0.73×10^{-4}	0.11×10^{-4}	0.38×10^{-5}	0.68×10^{-3}
0.40	32	0.45×10^{-1}	0.79×10^{-2}	0.28×10^{-2}	0.81×10^{-2}			
	64	0.45×10^{-1}	0.79×10^{-2}	0.15×10^{-2}	0.35×10^{-3}	0.91×10^{-3}		
	128	0.45×10^{-1}	0.79×10^{-2}	0.15×10^{-2}	0.30×10^{-3}	0.89×10^{-3}		

TABLE 1. Maximum absolute error in the free-surface velocitys $\Phi_z|_{z=\eta}$ of a Stokes wave of steepness ϵ for different values of mode number N and order of approximation M.

Table 1 shows the maximum absolute error in $\Phi_z|_{z=\eta}$ as a function of the order M and the maximum alias-free wavenumber N for a range of steepness ϵ, defined here for the Stokes wave as $\frac{1}{2}k(\eta_{\max}-\eta_{\min})$ where fundamental wavenumber $k=1$. It is clear that for the steepnesses $\epsilon \lesssim 0.35$, the error decreases exponentially fast with both N and M as they increase. (For any given M, the results converge to a limit exponentially rapidly as N is increased. On the other hand, N must be sufficiently large for the convergence with M to take place.) At $\epsilon = 0.40$, which is approximately 90 % of the Stokes limiting steepness, the expected convergence rate with respect to M is not realized. In fact, the solution diverges as M increases even if N is also increased so that the minimax error is only about 10^{-3}. In three dimensions, the maximum wave steepness that we are capable of using is likely to be smaller because more functional evaluations and higher wavenumbers $|\boldsymbol{\kappa}_N|$ are required. In practice, we first select M so that a given accuracy is achieved and then minimize N to limit round-off errors.

To evaluate the usefulness of the present method for long–short wave interactions, we also conduct these simple tests for a boundary-value problem given by the superposition of two Airy waves of wavenumbers k_{L} and $k_{\mathrm{S}}(k_{\mathrm{L}} \ll k_{\mathrm{S}})$ and amplitudes a_{L} and a_{S} respectively. The surface position is given by the linear elevation $\eta_{\mathrm{S}}+\eta_{\mathrm{L}}$, and the boundary condition Φ^{S} is prescribed by the analytic continuation of the linear potential to that surface. The boundary-value problem is solved for a range of $k_{\mathrm{S}}/k_{\mathrm{L}}$ and $k_{\mathrm{L}}a_{\mathrm{L}} = k_{\mathrm{S}}a_{\mathrm{S}}$. By again considering the maximum error in the vertical surface velocity, the exponential convergence with N and M for a given $\epsilon \approx k_{\mathrm{S}}a_{\mathrm{L}}$ is

		$T/\Delta t$				
ϵ	t/T	20	30	40	50	60
0.1	1	0.79×10^{-4}	0.16×10^{-4}	0.49×10^{-5}	0.19×10^{-5}	0.88×10^{-6}
	10	0.63×10^{-3}	0.12×10^{-3}	0.38×10^{-4}	0.15×10^{-4}	0.66×10^{-5}
0.2	1	0.30×10^{-3}	0.63×10^{-4}	0.21×10^{-4}	0.88×10^{-5}	
	10	0.28×10^{-2}	0.51×10^{-3}	0.16×10^{-3}	0.66×10^{-4}	

TABLE 2. Maximum absolute error in the free-surface elevation η of a progressive Stokes wave of steepness ϵ and period T after integration time t for different values of time step Δt.

confirmed. For example, for $k_S/k_L = 10$ and $k_L a_L = k_S a_S = 0.1$, we are able to recover six significant figures of accuracy for $M = 8$ and $N = 128$. If the steepness ϵ is doubled (keeping the same wavenumber ratios), however, the accuracy is decreased to only three decimal figures.

3.3.2. *Convergence of the numerical time integration*

We again use Stokes waves to evaluate the integration truncation error of our numerical scheme. The initial conditions for Φ^S and η are prescribed from an exact Stokes solution for a specified ϵ, and the wave is allowed to propagate across the computational domain. We consider the maximum absolute error in the surface elevation after time $t/T = 1$ and 10 for fundamental wave period T. No smoothing or filtering is used. Table 2 gives a summary of this error for a range of time-step sizes $\Delta t/T$ for $\epsilon = 0.1$ ($N = 16$, $M = 6$) and $\epsilon = 0.2$ ($N = 16$, $M = 8$). By examining the ratios of the errors as Δt is decreased, it is seen that the expected $O(\Delta t^4)$ global error is attained provided that the solution to the boundary-value problem is sufficiently accurate.

For our computations, the parameters M, N and Δt are chosen to give a desired accuracy (say $\delta \approx 10^{-5}$) using the following simple procedure: (i) select the order of the perturbation M so that $\delta \approx \epsilon^M$; (ii) choose the minimum number of Fourier modes N based on table 1 to realize the required accuracy; and (iii) choose $\Delta t/T$ according to table 2 subject to the linear Courant stability condition.

3.3.3. *Other accuracy checks*

For the numerical examples in §4, the accuracy of the results is checked for the conservation of volume and volume flux, and energy. For conservation of volume, we have

$$\int_{S_0} \eta \, d\boldsymbol{x} = \text{const}, \tag{3.6a}$$

where S_0 is the horizontal plane and the integral is easily evaluated in Fourier space. Alternatively, the total volume flux must be identically zero:

$$\int_{S_0} \eta_t \, d\boldsymbol{x} = 0, \tag{3.6b}$$

where η_t is given directly by (2.2). Equations (3.6) are typically maintained to within 10^{-5} in all the examples in §4. Finally, the solutions are evaluated for conserved total energy:

$$\int_{S_0} P_a \eta_t \, d\boldsymbol{x} = -\frac{1}{2}\frac{d}{dt}\left[\int_{S_0} \Phi^S \eta_t \, d\boldsymbol{x} + \int_{S_0} \eta^2 \, d\boldsymbol{x}\right]. \tag{3.7}$$

The first term is proportional to the rate at which work is done by the atmospheric pressure and the second term the rate of change of kinetic and potential energy in the fluid volume. If the surface pressure is zero, the total energy is constant. We remark that local measures of error such as smoothness are usually more useful for showing the loss of accuracy of a numerical scheme. Since we eliminate the high-wavenumber modes in our most nonlinear simulations, global checks such as energy conservation give a good measure of the cumulative effects.

4. Numerical results

To illustrate the validity and usefulness of the present method, we consider here four different numerical applications: (1) The steepening up to breaking of a Stokes wave due to an asymmetrically applied surface pressure. Our results are compared to those obtained using the fully nonlinear mixed-Eulerian–Lagrangian (MEL) method (Longuet-Higgins & Cokelet 1976; Vinje & Brevig 1981). (2) The evolution of a Stokes wavetrain due to type I unstable growth of sideband disturbances. Comparisons are made to the recent calculations of Stiassnie & Shemer (1987) using the modified Zakharov equations. (3) The long-time evolution of a Stokes wave packet. We study and make comparisons to experimental measurements of Su (1982). (4) Finally, to demonstrate the effectiveness of the method for large-scale problems, we consider the nonlinear interactions between two wave envelopes of different central frequencies as they collide. Although the wave packets themselves evolve considerably during the collision, even in the absence of the other group, the effect of the collision is not appreciable and as expected is manifested primarily as a shift in position as the groups emerge (Longuet-Higgins & Phillips 1962; Zakharov & Shabat 1972; Oikawa & Yajima 1974). We remark that for the long-time simulations, the problems may be more efficiently solved to lower orders or more approximately (say using only a few free-wave components) using the NLS or the Zakharov mode-coupling equations.

All the examples are in two dimensions and deep water using periodic boundary conditions. For simplicity, we fix the computational domain to be $-\pi \leqslant x \leqslant \pi$. The appropriate eigenfunction expansion is then (2.11) with $\boldsymbol{\kappa}_n = (n, 0)$, $n = 0, \pm 1, \pm 2, \ldots, \pm N$. The initial conditions are modulated Stokes waves which we prescribe from exact (14 decimals of accuracy) results. For later reference, we define $\Phi_0^{\mathrm{S}}[\epsilon, k]$ and $\eta_0[\epsilon, k]$ to be respectively the free-surface potential and elevation of a right-going Stokes wave of steepness ϵ and wavelength $\lambda = 2\pi/k$ whose phase is such that there is a crest at $x = -\pi$ at time $t = 0$.

4.1. *Steepening and breaking wave*

The present theory assumes from the outset that the free surface is single-valued, and, because of expansions of the potential about the mean position in (2.4), limited to waves that are not too steep (see §3.3). Our primary objective here is to study a wave that gradually steepens (and eventually overturns) and to consider how far our simulation can be continued before it fails. In addition to quantitative comparisons to fully nonlinear MEL calculations, it is also of interest to examine the behaviour of the solution and specifically the deviation in the energy conservation near the failure point. We use as initial condition a Stokes wave with $[\epsilon, k] = [0.15, 1]$ and apply a surface pressure, moving with the wave:

$$P_{\mathrm{a}}(x,t) = \begin{cases} P_0 \sin(2\pi t/T)\cos(x-ct), & 0 \leqslant t \leqslant \frac{1}{2}T, \\ 0, & t > \frac{1}{2}T, \end{cases} \tag{4.1}$$

MEL		Spectral method			
				No smoothing	With smoothing
$L = 32$	7.04	$N = 16$	$M = 4$	7.03	6.98
$L = 64$	7.11	$N = 16$	$M = 5$	7.15	7.10
$L = 128$	7.13	$N = 16$	$M = 6$	7.16	7.11
$L = 256$	7.14				

TABLE 3. Convergence in the maximum total energy ratio $E(\frac{1}{2}T)/E(0)$ of a Stokes wave with an applied asymmetric surface pressure. RK4 with $T/\Delta t = 100$ is used for all the calculations. For the case with smoothing, a five-point smoothing filter (3.2) is applied at every time step.

where T and c are respectively the fundamental period and phase speed of the Stokes wave, and $P_0 = 0.35$ for this simulation. The wave increases in energy until it reaches its maximum at $t = \frac{1}{2}T$ at which point the pressure is turned off. Table 3 shows the convergence of results for the ratio of the maximum total energy to the initial energy of the wave $E(\frac{1}{2}T)/E(0)$. The MEL formulation that we use is similar to that of Vinje & Brevig (1981). Cauchy's integral theorem is applied for this periodic deep-water case and the free surface is discretized into L linear segments with piecewise linear variation of the complex potential on each segment. For definiteness, no smoothing is used in the MEL calculation. For the present method, we consider both the case when there is no smoothing and when five-point smoothing (3.2) is applied at every time step. At $t = \frac{1}{2}T$, the wave has acquired a total energy over seven times its initial value. Even for this steep wave, the spectral method appears to converge rapidly as M increases ($N = 16$ already gives more than sufficient accuracy at $M = 6$). Hereinafter, we use $L = 64$ for MEL, and $N = 16$, $M = 6$ for the spectral-method calculations, and RK4 with $T/\Delta t = 100$ for all the time integrations.

In figure 1, we compare how well the numerical methods conserve energy as the wave evolves with time. Up to the point when the spectral method without smoothing fails, it conserves total energy better than the other two methods. The failure occurs at $t \approx 0.9T$ which is shortly after the kinetic energy of the wave has reached its maximum. The wave itself begins to turn over after the next maximum of the kinetic energy, and both the spectral method with smoothing as well as MEL (without smoothing) breakdown soon afterwards at $t \approx 1.5T$. In the spectral-method simulations, the amplitudes of the high-wavenumber modes increase as the wave steepens, and the final failure is marked by a change in the total energy due to a rapid growth of energy of the modes near the truncated end. An unrelated source of error is the saw-tooth instability which also affects the highest wavenumbers. Thus, our smoothing filters (3.2), (3.3) help to alleviate both problems.

Figure 2 plots the free-surface profiles using MEL and the spectral method (with smoothing) for two relatively late times $t/T = 0.96$ and 1.46. (The comparisons for earlier times are substantially better and the profiles cannot be distinguished graphically.) The comparisons are satisfactory over most of the wave profile with the main discrepancies occurring on the forward face, where the spectral-method slope is not as steep as that predicted by MEL, and at the crest as the wave steepens (and eventually overturns). For the spectral method, the maximum local wave slope reached is $(\partial\eta/\partial x)_{\max} \approx 0.9$ (six times the initial steepness) at $t \approx 1.05T$, at which point the total wave height is over three times its initial value.

The entire simulation (≈ 150 time steps) using the spectral method (with smooth-

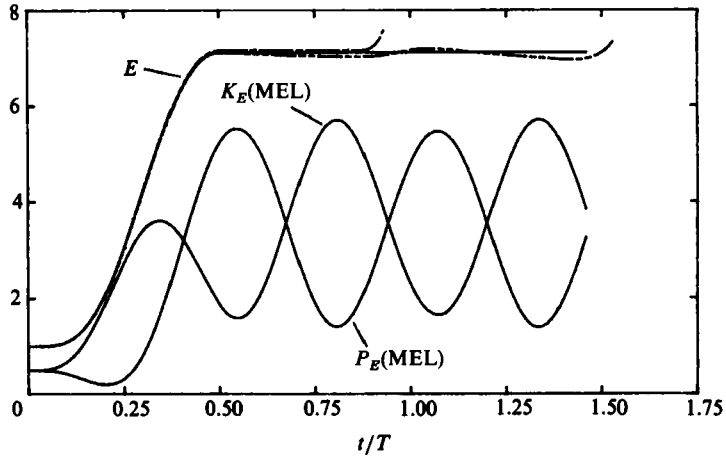

FIGURE 1. Ratios of the total energy E, potential energy P_E, and kinetic energy K_E relative to the initial total energy of a steepening wave (fundamental period T) under an asymmetric surface pressure. The results are for: ——, MEL; – – –, spectral method (without smoothing); – – – –, spectral method (with smoothing). The surface pressure is turned off after $t = \frac{1}{2}T$.

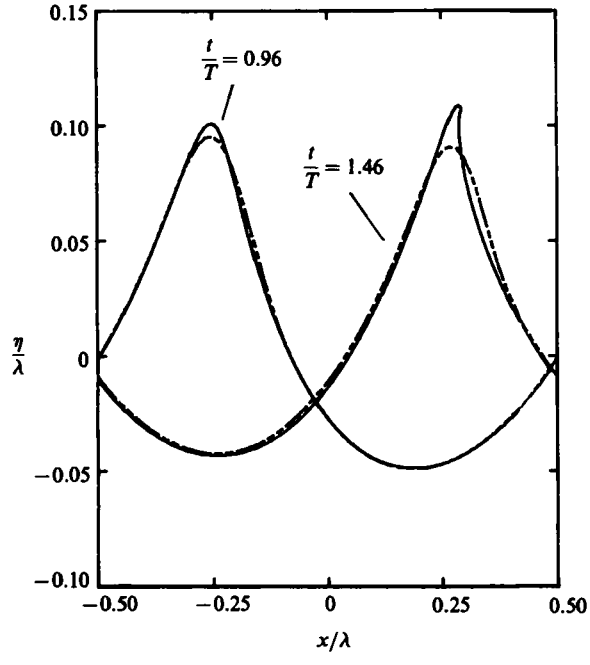

FIGURE 2. Free-surface profiles η of a steepening wave, fundamental period T and wavelength λ, under an asymmetric surface pressure calculated using MEL (——) and spectral method with smoothing (– – – –) at times $t/T = 0.96$ and 1.46. The vertical scale is exaggerated.

ing) for this problem with $N = 16$ and $M = 6$ requires less than half a minute of computation time on the Cray-2 computer. In contrast, the MEL computation with $L = 64$ takes approximately 20 times longer. More importantly, the computational effort for the spectral method increases only linearly with N and M, while the computation time for MEL, which has only a second-order accuracy, increases quadratically with the number of segments L.

4.2. *Modulation of a Stokes wavetrain due to type I instabilities*

Stiassnie & Shemer (1984) extended Zakarov's equation to fourth order, which they used in a later work (Stiassnie & Shemer 1987, hereinafter referred to as S&S) to simulate the coupled evolution of class I and class II instabilities of surface gravity waves on deep water. In this section, we compare our spectral-method calculations to their simulation for type I instability of a Stokes wavetrain. For their Airy wave steepness of $\epsilon_0 = (\kappa a)_0 = 0.13$, the wavenumbers of the most unstable class I modes are approximately $\pm 22\,\%$ of the fundamental. In order to make a comparison, we use as initial condition a Stokes wave, $[\epsilon, k] = [0.13, 9]$, modulated by two Airy sideband waves ($k = 9$ is chosen so that integral numbers of the sideband modes can be fitted into the computational domain):

$$\left.\begin{aligned} \eta(x,0) &= \eta_0[0.13,9] + 0.1a_0\cos(7x - \tfrac{1}{4}\pi) + 0.1a_0\cos(11x - \tfrac{1}{4}\pi), \\ \Phi^S(x,0) &= \Phi_0^S[0.13,9] + 0.1\frac{a_0}{\sqrt{7}}e^{7\eta}\sin(7x - \tfrac{1}{4}\pi) + 0.1\frac{a_0}{\sqrt{11}}e^{11\eta}\sin(11x - \tfrac{1}{4}\pi), \end{aligned}\right\} \quad (4.2)$$

which to leading order is the same as that used by S&S. In S&S's fourth-order simulation, only a limited approximation with 5 free waves was used. To compare with S&S, we set $M = 4$ but consider a total of $N = 64$ free wave modes. Our time step is $\frac{1}{50}$ of the fundamental wave period T, and no smoothing filter is used.

The time histories of the fundamental ($k = 9$), subharmonic ($k = 7$), and superharmonic ($k = 11$) are plotted in figure 3 and compared to S&S's results (their figure 1). Both computations predict a first minimum of the fundamental near $t \approx 60T$, which closely corresponds to the timescale for type I interactions, T/ϵ_0^2. The amplitude of each harmonic relative to the initial amplitude of the fundamental does not agree as well, but the overall qualitative behaviour (for example the relative amplitudes of the two side harmonics at their maximum and minimum) is preserved.

Unlike S&S, our simulation breaks down after $t \approx 140$, at which time the wave steepens and possible local breaking phenomena cannot be ruled out. This is further indicated by the conservation of total energy for our run which is shown in figure 4 for the quantity $(E(t/T) - E(0))/E(0)$. Our total energy is conserved to within 0.01 % for $t < 40T$, to within 0.1 % for $t < 50T$, and to within 2 % for the duration of the simulation. (For comparison, S&S reported total energy conserved to within 1 %.) Near $t \approx 60T$, which corresponds to the minimum of the fundamental amplitude and maxima of the sideband amplitudes, there is an abrupt change (of the order of 0.5 %) in the total energy, after which the numerical result recovers but eventually breaks down at $t \approx 140$, which again corresponds to maxima in the sideband perturbations.

Figure 5 shows the actual free-surface elevations at times $t/T = 0$, 57 and 104. At $t/T = 0$ and 104, the fundamental dominates, while at $t/T = 57$ the sidebands do. The maximum local wave slope reaches almost four times ($(\partial\eta/\partial x)_{\max} \approx 0.6$) that of the initial wave at $t = 57T$, which may suggest why the computed total energy is not as well conserved near that time.

4.3. *Evolution of a wave packet – comparison to experimental measurements*

Su (1982) studied experimentally the evolution of wave groups that had initially square envelopes. For (Airy) wave steepnesses ranging from $\epsilon_0 = 0.09$ to 0.28, he measured the free-surface elevation at eight stations down the tank. For wave steepnesses $\epsilon_0 \geqslant 0.14$, he observed intense two-dimensional breaking at distances between ten and twenty carrier wavelengths from the wavemaker. Fifteen to

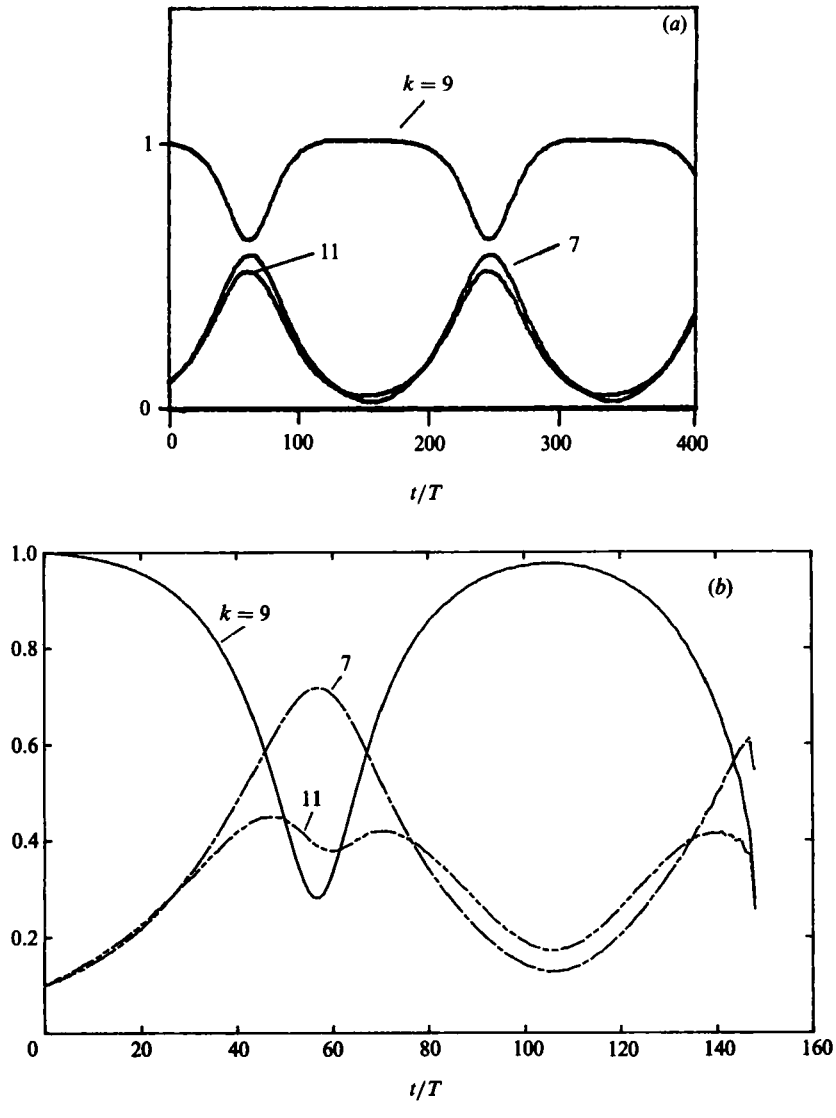

FIGURE 3. Time histories of the amplitudes of the fundamental ($k = 9$), subharmonic ($k = 7$) and superharmonic ($k = 11$) modes relative to the initial amplitude of the fundamental for an evolving Stokes wavetrain. (*a*) From Stiassnie & Shemer (1987); (*b*) present results. T is the period of the fundamental.

twenty-five wavelengths from the wavemaker, crescent-shaped breaking waves often developed, and from twenty to forty-five wavelengths away, two-dimensional spilling breaking was common. In this section, we compare our theory to one of Su's experiments, which initially had a steepness of $\epsilon_0 = 0.15$ and a packet which contained approximately five fundamental waves at the beginning. To simulate this experiment, we begin with a Stokes wavetrain which has 15 waves in the computational domain, i.e. $[\epsilon, k] = [0.15, 15]$, and modulate it with a tapering function of the form

$$F(x; \sigma, x_b, x_e) = 0.5\{\tanh[\sigma(x - x_b)\} - \tanh[\sigma(x - x_e)]\}. \tag{4.3}$$

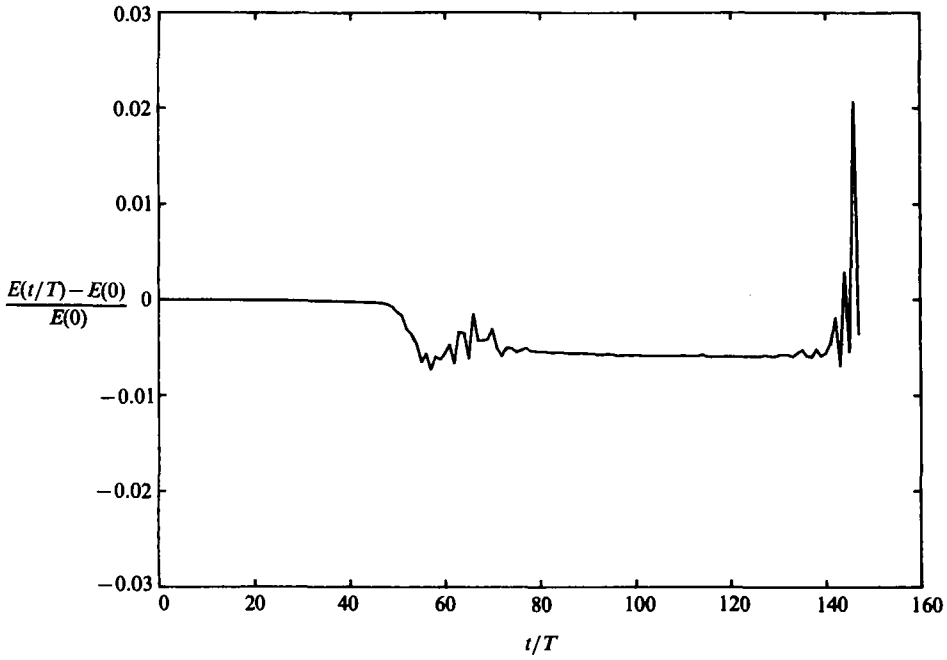

FIGURE 4. Relative change in the spectral-method total energy $(E(t/T)-E(0))/E(0)$, of an evolving Stokes wavetrain, fundamental period T.

The parameter σ measures the steepness of the taper at the beginning and end positions, x_b and x_e respectively, of the resulting envelope. To avoid Gibb's phenomenon at the boundaries, (4.3) is periodically extended. The initial condition that approximately gives the desired five waves in the packet is then

$$\left.\begin{aligned}\eta(x,0) &= F\left(x;\frac{30}{\pi},-\frac{\pi}{3},\frac{\pi}{3}\right)\eta_0[0.15,15],\\ \Phi^S(x,0) &= F\left(x;\frac{30}{\pi},-\frac{\pi}{3},\frac{\pi}{3}\right)\Phi_0^S[0.15,15].\end{aligned}\right\} \tag{4.4}$$

(Note that a wave probe would measure ten waves in (4.4) since the group velocity is roughly half the phase velocity in deep water.) The parameters for our numerical simulation are $N = 256$, $M = 6$ and $T/\Delta t = 40$. To allow the computations to continue after the waves may have become locally too steep, and possibly also to model some loss of wave energy due to breaking, we apply the ideal filter Λ_I with $\nu = 0.5$ whenever the total energy of the wave packet changes by more than 1 %. This smoothing operation eliminates all Fourier modes whose wavenumbers are greater than eight times the fundamental.

We show comparisons between Su's wave-probe measurements and our computed results in figure 6. The experimental traces are reproduced directly from Su (1982) and do not have a vertical scale. The horizontal scales are, however, the same. Overall, the agreement is qualitatively good and appears to improve as the wave group travels down the tank. At about fifty wavelengths from the wavemaker, we confirm the experimental observation that the wave group fissions into two packets. In comparison to the computations for the same experiment by Lo & Mei (1985), who used Dysthe's fourth-order NLS, our results are comparable.

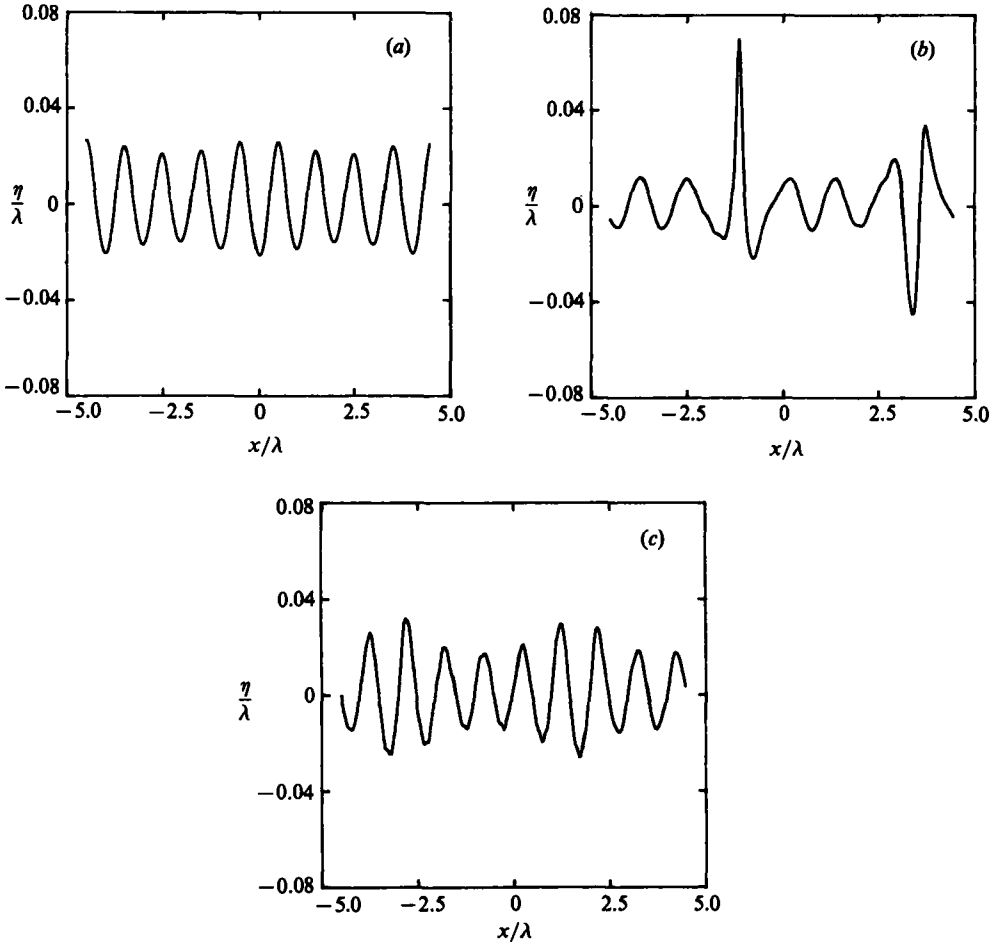

FIGURE 5. Instantaneous free-surface elevation of an evolving Stokes wavetrain (fundamental period T and wavelength λ) at times: (*a*) $t/T = 0$; (*b*) 57; and (*c*)104. The vertical scales are exaggerated.

The total-energy time history is shown in figure 7. The energy is conserved well except at approximately $t/T \approx 40$–50. In this region, the filter $\Lambda_{\mathrm{I}}(k, 0.5)$ (triggered by a 1 % change in energy) is repeatedly applied, which eventually removed almost 20 % of the energy from the system. We find that filtering (singly or in close succession) is often required at intervals of approximately two fundamental periods, which may be related to the relative motion between the waves and their envelope as suggested by Longuet-Higgins (1974). It is interesting to note that the time range over which we use smoothing roughly corresponds to times at which wave breaking was observed in the experiments. By monitoring the total energy and suitably removing energy in the higher-wavenumber modes, the present method can be continued beyond the stages of apparent local breaking. In many applications, this may offer an advantage over fully nonlinear methods such as MEL, which breakdown as soon as the wave begins to spill or plunge into itself.

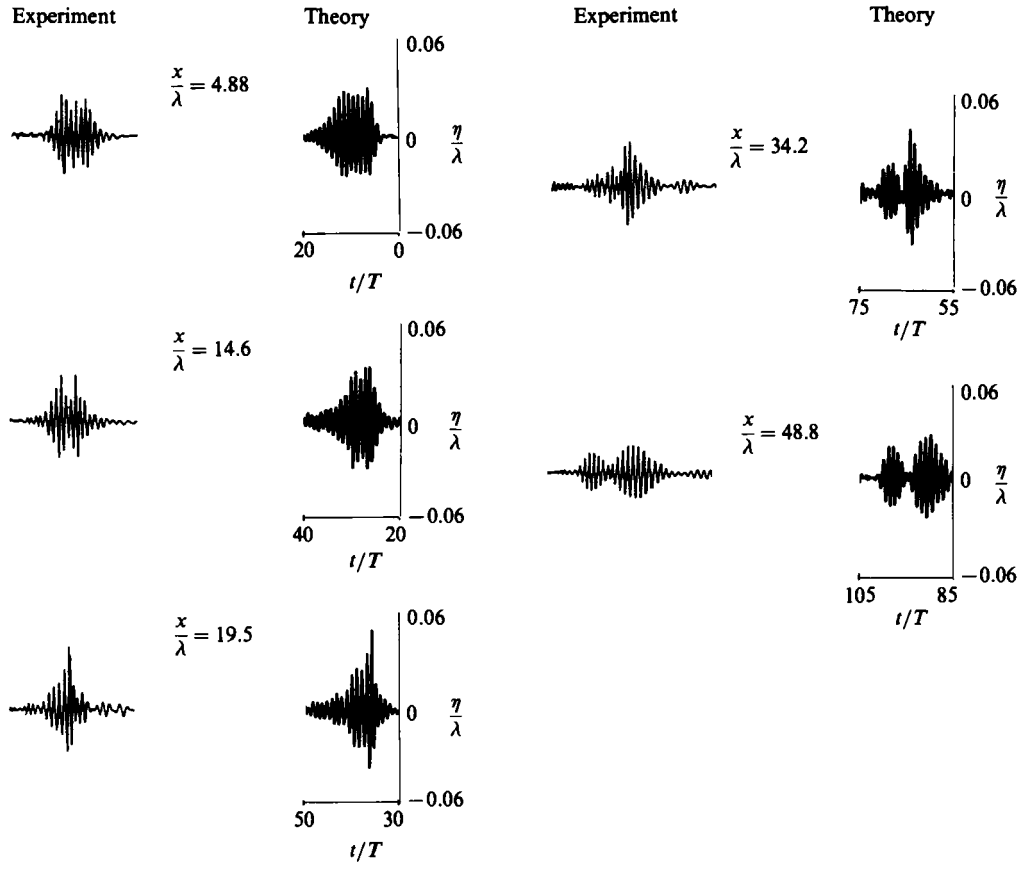

FIGURE 6. Comparison between experiments and theory for the free-surface elevation of an evolving wave packet (fundamental period T and wavelength λ) at positions from the wavemaker $x/\lambda = 4.88$, 14.6, 19.5, 34.2 and 48.4. The experimental results are reproduced from Su (1982).

4.4. *Nonlinear interactions between two wave groups*

This example is chosen primarily to demonstrate the performance of the present method for a larger-scale problem. We consider the head-on collisions between two wave groups for which the wavelength of the waves in one group is twice that of the other. For each wave group, the initial steepness of the waves is $\epsilon = 0.16$. To evaluate the effect of the inter-group interactions, we repeat each simulation with only a single propagating group present and compare the results. In the nonlinear simulations, we use $N = 512$, $M = 6$, and $T_S/\Delta t = 40$, where T_S is the fundamental period of the shorter waves. The ideal smoothing filter Λ_I with $\nu = 0.9$ is used every forty time steps or one short-wave period. The total energy is conserved to five significant figures for the duration of the simulations. As initial conditions we choose

$$\left.\begin{aligned} \eta(x,0) &= F\left(x;\frac{25}{\pi},-\frac{9\pi}{25},-\frac{3\pi}{25}\right)\eta_0[0.16,50]+F\left(x;\frac{25}{2\pi},\frac{6\pi}{25},\frac{18\pi}{25}\right)\eta_0[0.16,25], \\ \Phi^S(x,0) &= F\left(x;\frac{25}{\pi},-\frac{9\pi}{25},-\frac{3\pi}{25}\right)\Phi_0^S[0.16,50]-F\left(x;\frac{25}{2\pi},\frac{6\pi}{25},\frac{18\pi}{25}\right)\Phi_0^S[0.16,25], \end{aligned}\right\} \quad (4.5)$$

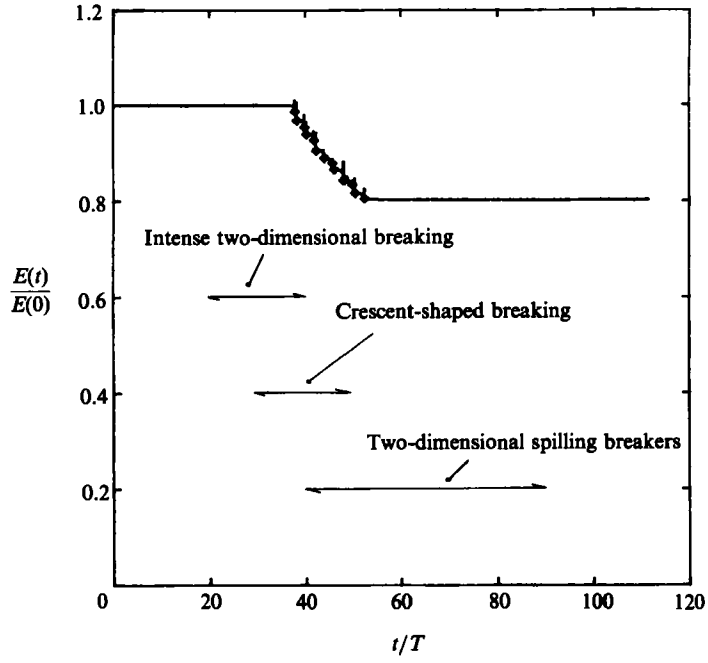

FIGURE 7. Computed total energy of an evolving wave packet, fundamental period T and wavelength λ. Diamond symbols indicate the use of the ideal filter $\Lambda_1(\nu = 0.9)$ which is applied whenever the total energy changes by more than 1 %.

which gives approximately six waves in each group. Figure 8(*a*) shows this initial profile together with its Hilbert transform envelope $A(x,t)$ given by

$$A^2(x,t) = \eta^2(x,t) + H^2(\eta(x,t)). \tag{4.6}$$

The fingering in the envelope is caused by the wave crests being more peaked than the troughs. Figure 8 shows the free-surface profiles after the interaction has taken place at $t = 31T_S$ when the groups have emerged on the opposite sides. These are compared to the single groups after propagating for the same time, and to the linear result (for the short-wave envelope in figure 8*c*) obtained using $M = 1$ and the same N and Δt. The interaction time is smaller than, but of the same order as, that required for type I interactions $\approx T_S/\epsilon_0^2 = 39T_S$. As expected, the interaction between the groups is relatively small even though the effects of nonlinearity are appreciable as shown by the steepened fronts and the characteristic wedge-like shapes of the individual envelopes (e.g. Su 1982). Even with sixth-order interactions included, the only effect of the collision appears to be a small shift in position of the envelope corresponding to a decrease in speed of the group. The effect is more pronounced for the short-wave group, which is in qualitative agreement with the predictions of Longuet-Higgins & Phillips (1962) for decreases in phase speeds of two third-order Stokes wavetrains travelling in opposite directions. The present results generalize to higher order the observations of Oikawa & Yajima (1974) for interacting solitons of different carrier frequencies.

This research was financially supported by the National Science Foundation (NSF Grant MEA 8210647) and the Office of Naval Research (Contract N00014-82-K-0198). Most of the computations were performed on the Minnesota Supercomputer Institute

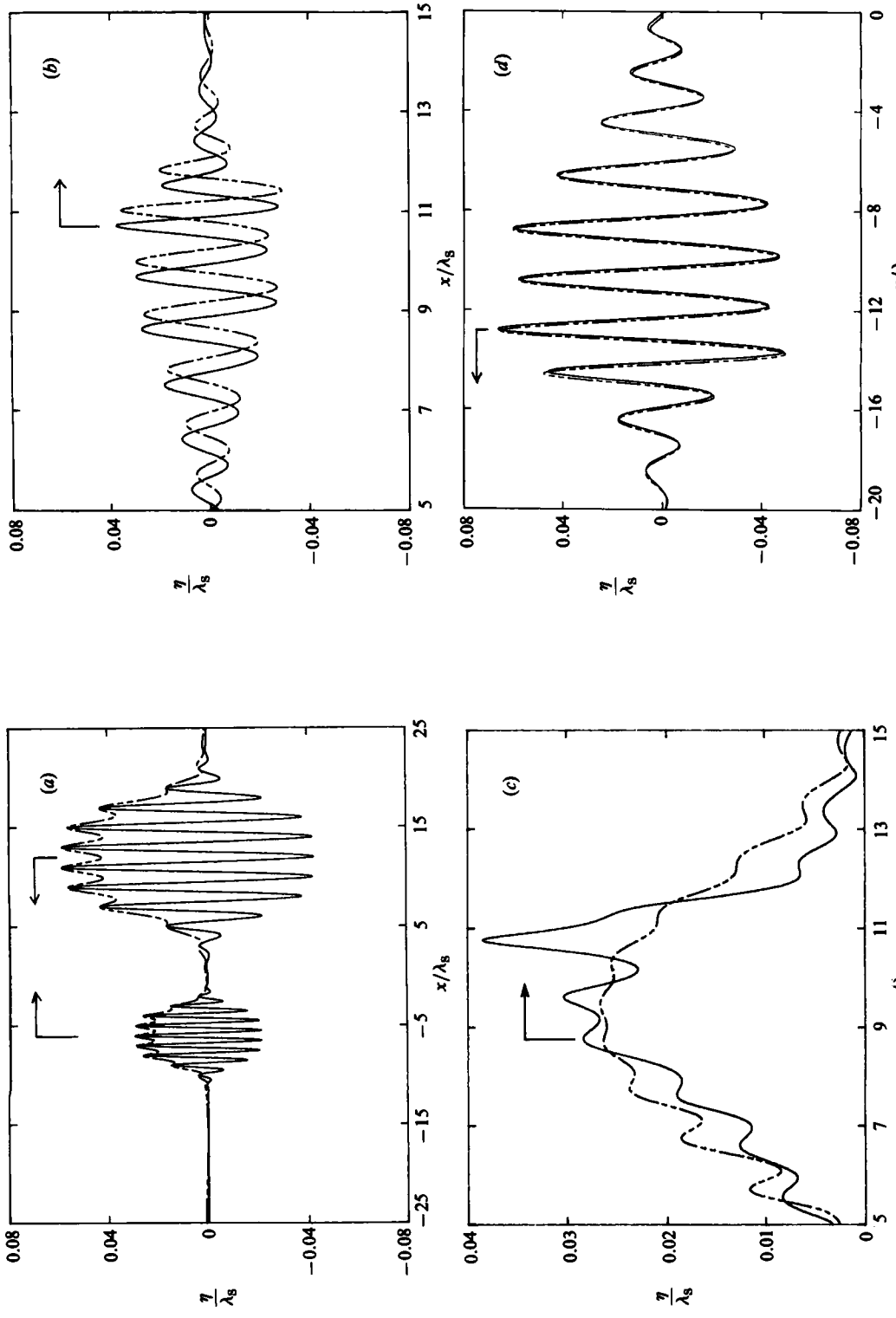

FIGURE 8. Free-surface elevations of two colliding wave packets of different carrier periods T_L and T_S, and wavelengths λ_L and λ_S with $\lambda_L = 2\lambda_S$. (*a*) Initial profiles ($t/T_S = 0$) before collision (——) and their Hilbert-transform envelopes (– – – –). (*b*) Final surface profile ($t/T_S = 31$) of the short-wave group (——) compared to one which has evolved independently (– – – –). (*c*) Hilbert-transform envelope of the final surface profile ($t/T_S = 31$) of the short-wave group (——), compared to that from linearized theory (– – – –). (*d*) Final surface profile ($t/T_S = 31$) of the long-wave group (——) compared to one that has evolved independently (– – – –). The vertical scales are exaggerated.

Cray-2 and the John von Neumann Center Cyber-205 computers, both under the sponsorship of NSF.

REFERENCES

BENNEY, D. J. 1962 Nonlinear gravity wave interactions. *J. Fluid Mech.* **14**, 577–589.

BRYANT, P. J. 1983 Cyclic gravity waves in deep water. *J. Austral. Math. Soc.* B **25**, 2–15.

COHEN, B. I., WATSON, K. M. & WEST, B. J. 1976 Some properties of deep water solitons. *Phys. Fluids* **19**, 345–354.

CRAWFORD, D. R., LAKE, B. M., SAFFMAN, P. G. & YUEN, H. C. 1981 Stability of weakly nonlinear deep-water waves in two and three dimensions. *J. Fluid Mech.* **105**, 177–191.

DOLD, J. W. & PEREGRINE, D. H. 1986 An efficient boundary-integral method for steep unsteady water waves. In *Numerical Methods for Fluid Dynamics II* (ed. K. W. Morton & M. J. Baines), pp. 671–679. Oxford University Press.

DYSTHE, K. B. 1979 Note on a modification to the nonlinear Schrödinger equation for application to deep water waves. *Proc. R. Soc. Lond.* A **369**, 105–114.

FORNBERG, B. & WHITHAM, G. B. 1978 A numerical and theoretical study of certain nonlinear wave phenomena. *Phil. Trans. R. Soc. Lond.* A **289**, 373–404.

LO, E. & MEI, C. C. 1985 A numerical study of water-wave modulation based on a higher-order nonlinear Schrödinger equation. *J. Fluid Mech.* **150**, 395–416.

LONGUET-HIGGINS, M. S. 1974 Breaking waves in deep or shallow water. In *Proc. 10th Symp. Naval Hydro.*, Cambridge, Mass. (ed. R. D. Cooper & S. W. Doroff), pp. 597–605. Government Printing Office, Washington.

LONGUET-HIGGINS, M. S. & COKELET, E. D. 1976 The deformation of steep surface waves on water. I. A numerical method of computation. *Proc. R. Soc. Lond.* A **350**, 1–26.

LONGUET-HIGGINS, M. S. & PHILLIPS, O. M. 1962 Phase velocity effects in tertiary wave interactions. *J. Fluid Mech.* **12**, 333–336.

MARTIN, D. U. & YUEN, H. C. 1980 Quasi-recurring energy leakage in the two-space-dimensional nonlinear Schrödinger equation. *Phys. Fluids* **23**, 881–883.

OIKAWA, M. & YAJIMA, N. 1974 A perturbation approach to nonlinear systems. II. Interaction of nonlinear modulated waves. *J. Phys. Soc. Japan* **37**, 486–496.

ORSZAG, S. A. 1971 Numerical simulation of incompressible flows within simple boundaries: accuracy. *J. Fluid Mech.* **49**, 75–112.

PHILLIPS, O. M. 1960 On the dynamics of unsteady gravity waves of finite amplitude. Part 1. The elementary interactions. *J. Fluid Mech.* **9**, 193–217.

RIENECKER, M. M. & FENTON, J. D. 1981 A Fourier approximation method for steady water waves. *J. Fluid Mech.* **104**, 119–137.

SCHWARTZ, L. W. 1974 Computer extension and analytic continuation of Stokes' expansion for gravity waves. *J. Fluid Mech.* **62**, 553–578.

STIASSNIE, M. & SHEMER, L. 1984 On modifications of the Zakharov equation for surface gravity waves. *J. Fluid Mech.* **143**, 47–67.

STIASSNIE, M. & SHEMER, L. 1987 Energy computations for evolution of class I and class II instabilities of Stokes waves. *J. Fluid Mech.* **174**, 299–312.

SU, M. Y. 1982 Evolution of groups of gravity waves with moderate to high steepness. *Phys. Fluids* **25**, 2167–2174.

VINJE, T. & BREVIG, P. 1981 Nonlinear ship motions. *Proc. 3rd Intl Symp. Num. Ship Hydro.*, Paris.

WEST, B. J. 1982 Statistical properties of water waves. Part 1. Steady-state distribution of wind-driven gravity–capillary waves. *J. Fluid Mech.* **117**, 187–210.

WEST, B. J., WATSON, K. M. & THOMSON, A. J. 1974 Mode coupling description of ocean wave dynamics. *Phys. Fluids* **17**, 1059–1067.

WHITHAM, G. B. 1974 *Linear and Nonlinear Waves.* Wiley.

YUEN, H. C. & FERGUSON, W. E. 1978 Fermi–Pasta–Ulam recurrence in the two-space dimensional nonlinear Schrödinger equation. *Phys. Fluids* **21**, 2116–2118.

YUEN, H. C. & LAKE, B. M. 1982 Nonlinear dynamics of deep-water gravity waves. *Adv. Appl. Mech.* **22**, 67–229.

ZAKHAROV, V. E. 1968 Stability of periodic waves of finite amplitude on the surface of a deep fluid. *J. Appl. Mech. Tech. Phys.* **9**, 190–194. (English Translation.)

ZAKHAROV, V. E. & SHABAT, A. B. 1972 Exact theory of two-dimensional self-focusing and one-dimensional self-modulation of waves in nonlinear media. *Sov. Phys., J. Exp. Theor. Phys.* **34**, 62–69.